A traveling wave X-band accelerating structure with low-beta front end for a compact inverse Compton scattering x-ray source.

Xavier F. D. Stragier[1,2*], Alexej Grudiev[2], Daniel Nijhof[1], Thomas G. Lucas[1,3], Ids van Elk[1], Coen Sweers[1], Peter Mutsaers[1], Rolf Wegner[2], Nuria Catalan Lasheras[2], Walter Wuensch[2], Jom Luiten[1*]

[1*]Department of Applied physics, Eindhoven University of Technology, P.O. Box 513, Eindhoven, 5600 MB, Netherlands.
[2]CLIC, CERN, Espl. des Particules 1, Genève, 1217, Switzerland.
[3]Paul Scherrer Institute, Villigen, 5232, Switzerland.

*Corresponding author(s). E-mail(s): x.f.d.stragier@tue.nl; o.j.luiten@tue.nl;

Abstract

Smart*Light is a table-top inverse Compton scattering X-ray source under development at Eindhoven University of Technology. The linac-based source aims for a very compact design through the use of X-band technology operating at accelerating gradients exceeding 60 MV/m. The heart of the linac is an X-band accelerating structure whose design is based on the T24 structure developed as a prototype for the Compact Linear Collider. To allow for the capture and acceleration of sub-relativistic electron bunches to energies of $\sim$ 30 MeV two adjustments have been made to the structure: the first is a reduction in the length of the first cells to match the injected particle velocities, and the other is to add additional cells to efficiently use RF power that would otherwise be dissipated within a load. Here we present the design, manufacturing, and commissioning of the Smart*Light X-band accelerating structure.

Keywords: inverse Compton scattering, x-ray source, X-band, linear accelerator, high gradient electric field.

1 Introduction

X-rays allow us not only to look *through* but also *inside* material objects and determine their structural, elemental, and even chemical composition with very high spatial resolution in a relatively non-destructive way. For this reason, x-ray analysis has become an indispensable tool in, for example, medical diagnostics, industrial production lines, cultural heritage, life sciences, and materials science. However, the most advanced x-ray analytical methods require highly brilliant x-ray beams with continuously tunable photon energies, which are only available at synchrotron light sources or Free-Electron Lasers (FEL) [1]. These large-scale facilities are unfortunately scarce and their precious beam-time has to be shared by many users. Moreover, since their use requires travel, application in industries such as manufacturing, medicine or the arts is largely excluded. For many years the only alternative was provided by x-ray tubes [2], which are undeniably low-cost and very compact but only generate x-ray photons at characteristic wavelengths of the anode material at a brilliance many orders of magnitude lower than what can be offered by synchrotrons and FELs. In recent developments, the brilliance of x-ray tube-based sources has been significantly improved by utilizing a liquid metal as anode material [3] and the x-ray spectrum offered has been increased by a clever combination of multiple anode materials in a single device [4]. However, a single narrow-band table-top x-ray source of sufficient brilliance, providing continuously tuneable photon energies across the entire x-ray spectrum is not available yet.

1.1 ICS x-ray sources

A relatively new development is the inverse Compton scattering (ICS) x-ray source, which is based on Compton scattering of intense laser pulses by relativistic electrons, as is illustrated in Fig. (1). An electromagnetic wave with wavelength λ_L, propagating under an angle θ_L with respect to the negative z-axis, and colliding with an electron traveling along the positive z-axis with velocity $\mathbf{v} = \beta c\hat{z}$, will be (partially) scattered under an angle θ_X with respect to the positive z-axis. Due to the relativistic Doppler effect, the scattered light has a wavelength of

$$\lambda_\mathrm{X} = \lambda_\mathrm{L} \frac{1 - \beta\cos\theta_\mathrm{X}}{1 + \beta\cos\theta_\mathrm{L}}. \tag{1}$$

For ultra-relativistic speeds ($\beta \approx 1$) and small angles ($\theta_{\mathrm{X,L}} \ll 1$) Eq. (1) can be approximated by

$$\lambda_\mathrm{X} \approx \frac{\lambda_\mathrm{L}}{4\gamma^2}(1 + \gamma^2\theta_\mathrm{X}^2), \tag{2}$$

with $\gamma \equiv 1/\sqrt{1-\beta^2} \gg 1$ the Lorentz factor. As an example, an electron bunch with an energy of 25 MeV, corresponding to $\gamma \approx 50$, which is colliding head-on with a counter-propagating laser pulse, would give rise to scattered photons with a wavelength λ_X which is $4\gamma^2 \approx 10^4$ times shorter than the laser wavelength λ_L, i.e. well into the hard x-ray regime. Such electron bunch energies can be realized straightforwardly with a table-top linac. Importantly, a bandwidth of the order of a few percent can be realized by selecting a small part of the emission cone, i.e., $\theta_\mathrm{X} \ll \gamma^{-1}$, (see Eq. (2)) and the

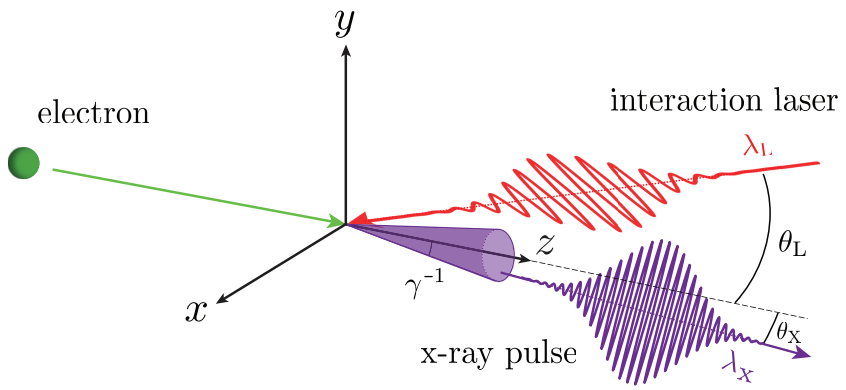

Fig. 1 A laser pulse with wavelength λ_L, hitting an electron traveling in the z-direction with velocity $\mathbf{v} = \beta c\hat{z}$, generates light by Compton scattering with wavelength λ_X. For highly relativistic electron velocities ($\beta \approx 1$) the scattered light has a wavelength λ_X in the x-ray range and is confined to a narrow cone with half angle $\sim \gamma^{-1}$, centered around the z-axis.

x-ray energy can be tuned continuously by changing either the electron bunch energy (see Eq. (2)) or the angle θ_L of the laser pulse (see Eq. (1)).

The scattering process is governed by the (extremely small) Thomson cross section $\sigma_T = 8\pi r_0^2/3$, where $r_0 = e^2/(4\pi\epsilon_0 mc^2) \approx 2.82\,\mathrm{fm}$ is the classical electron radius, with m the electron rest mass. To realize a flux of x-ray photons which is sufficient for actual applications, high-intensity laser pulses should collide with high-charge electron bunches in the smallest possible spot size at the highest possible repetition rate. If the laser pulse length and the electron bunch length are much shorter than the depth of focus of both beams, the number of x-ray photons N_X generated by a single electron bunch-laser pulse collision is given by

$$N_X = \sigma_T \frac{N_e N_L}{2\pi(\sigma_e^2 + \sigma_L^2)}, \tag{3}$$

where N_e is the number of electrons per bunch, N_L the number of photons per laser pulse, σ_e the rms radius of the electron bunch, and σ_L the rms radius of the laser pulse in the interaction point.

There are two approaches to ICS x-ray sources: linac-based [5–8], allowing only a single pass of each electron bunch to generate x-rays; and storage-ring-based [9, 10], in which the electron bunches can be recycled many times. Storage-ring-based sources enable higher repetition rates and therefore higher average x-ray photon fluxes. Linac-based systems, however, typically feature electron bunches with a lower emittance, enabling a smaller interaction spot size σ_e and therefore a higher x-ray beam coherence. Furthermore, Linac-based systems feature the possibility of changing the energy of the produced x-ray form shot-to-shot by adjusting the electron bunch energy in between RF pulses. This can be done by adjusting the phase or/and the power of the RF pulses. Changing the electron energy in a storage-ring-based ICS on the other hand, requires adjustment of the magnetic elements in the ring, which takes minutes to hours to vary and stabilize.

1.2 Smart*Light

In the Smart*Light project at Eindhoven University of Technology (TU/e) a linac-based ICS source is being developed. The main drive behind the project is to realize an x-ray source that can provide advanced x-ray analytical techniques that cannot be offered by conventional x-ray tubes, while still being sufficiently small and affordable to be installed in university laboratories, industry, museums and hospitals. Since compactness is central to the design criteria, we opted for a linac-based device that uses X-band traveling wave accelerating structures. This has the additional advantage that it can be run at high repetition rates, which is essential to achieve a sufficiently high average brilliance. The first X-band accelerating structure in the linac is a modified version of the T24-cell CLIC (Compact LInear Collider) accelerating structure developed at CERN. In the current layout, this X-band accelerating structure stands alone in the linac. However, the modular nature of linacs allows for additional unmodified accelerating structures to be added, to reach higher electron beam energies. Recently, first light was obtained in the Smart*Light project [11]. In this paper, we focus on the design, manufacturing, and commissioning of this first accelerating structure of the X-band linac.

This paper organized as follows: In Sect. 2 we describe the entire design and manufacturing process of the X-band accelerating structure. For conciseness, we will refer to our new X-band traveling-wave accelerating structure as simply the X-band structure. In Sec. 2.1.1 we first discuss the specific demands the accelerator has to meet for this particular application. In Sec. 2.1.2 the demands are translated into an actual design of an X-band structure, which is optimized following a comprehensive optimization procedure of the various design parameters. In Sec. 2.2 the manufacturing and tuning of the X-band structure is described in some detail. Subsequently, in Sec. 3, the conditioning of the X-band structure is treated, which started after integration of the X-band structure into the Smart*Light beamline. The conditioning process is still ongoing but we can already accelerate electrons to sufficiently high energies for the generation of hard x-rays by inverse Compton scattering. In Sec. 4 an example of a measured ICS x-ray spectrum is presented and analyzed, showing that the X-band structure operates as expected. In Sec. 5 we end with concluding remarks.

2 Design and manufacturing of the X-band structure

In the following section we will first focus on the design process of the X-band structure and subsequently on the manufacturing of the device.

2.1 Design of the traveling wave X-band structure

2.1.1 Design considerations

The goal of the Smart*Light project is to develop a compact ICS x-ray source that produces narrow-band x-rays with photon energies that can be continuously tuned from $\sim$ 1 keV to at least 20 keV. To produce the desired x-ray photon energies, a 1 kHz, 10 mJ, 100 fs, 800 nm amplified Ti:Sapphire laser system is used. It folows from Eq. (2) that electron kinetic energies up to $E_{\mathrm{kin}}(\gamma - 1)mc^2 \approx 30\,\mathrm{MeV}$ are required.

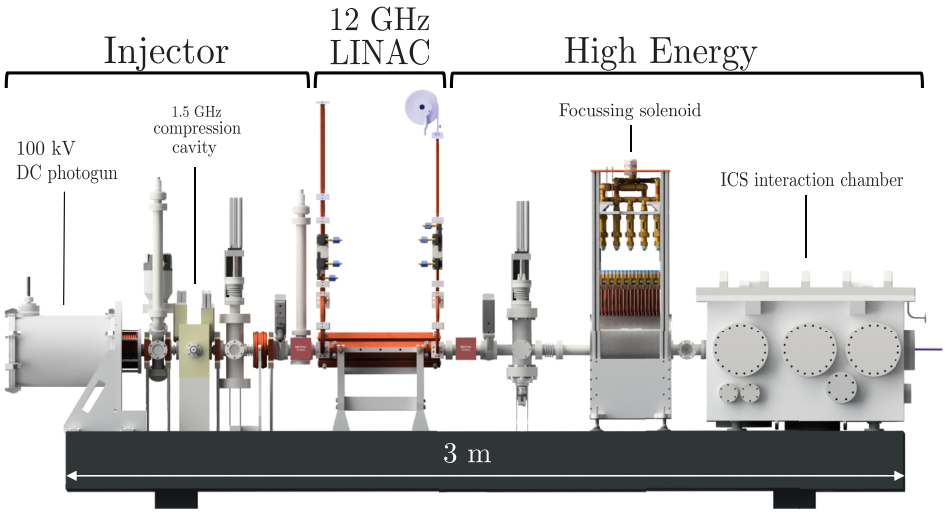

Fig. 2 Side view of the complete electron beamline including laser-electron interaction chamber. The main components of the beamline are indicated. The distance from the cathode in the DC photogun to the interaction point with the laser is 2.2 m [16].

The complete electron beamline should preferably fit on a standard 3 m optical table (See Fig. 2). Taking into account the space requirements of the electron injector, the focusing solenoids, the electron-laser interaction chamber and various electron and laser beam diagnostics, this leaves about 0.5 m for the linac. This implies a minimum required effective acceleration gradient of $\sim$ 60 MV/m in the linac. On the one hand, to maximize the number of x-ray photons generated per second, the repetition rate of the accelerator should be as high as possible. For reliability, on the other hand, the breakdown rate of the accelerator has to be as low as possible. To achieve high-gradient electron acceleration at high repetition rates and low breakdown rates, the CLIC X-band technology was chosen [12–14] for the Smart*Light project. The CLIC accelerating structures operate at a frequency of 11.9942 GHz and are designed to generate an average on-axis gradient of 100 MV/m. A single 6 MW klystron in combination with an RF pulse compressor can produce 24 MW RF pulses. By feeding these pulses into a CLIC X-band accelerating structure, an average on-axis acceleration gradient of 70 MV/m can be realized, at a repetition rate of 400 Hz [15]. These properties are in line with the requirements for the Smart*Light project.

It was decided to use a 'low' voltage 100 kV DC photogun as injector instead of a more conventional RF photogun because it is very compact (see Fig. 2) and can be operated at a much higher repetition rate ($>$ 1 kHz). Additional reasons are the user-friendliness of the small 100 kV DC power supply compared to a klystron/modulator system required for an RF photogun and the overall reliability, robustness and proven performance of the DC photogun. The photogun was originally designed and developed at TU/e for 100 fs, single-shot, ultra-fast electron diffraction experiments [17–21]. It features a 10 MV/m DC acceleration field, allowing the extraction of ultra-short electron bunches with charges up to 100 pC, which are produced by photoemission

from the copper cathode using 266 nm femtosecond UV laser pulses. The UV pulses are created by third-harmonic generation of 800 nm, 100 fs laser pulses, that are split off from the main Ti:Sapphire femtosecond laser pulse and therefore automatically synchronized to the Compton scattering interaction laser pulses.

A distinct disadvantage of electron injection at the sub-relativistic energy of 100 keV is the relatively fast Coulomb expansion of the bunch directly after creation, not strongly mitigated by relativistic effects. For this reason a velocity buncher cavity, operating at 1.5 GHz in the TM_{010} mode, is installed between the DC photogun and the X-band structure, counteracting Coulomb expansion by longitudinally compressing the electron bunch to the picosecond level at the entrance of the X-band structure [18, 19]. This ensures that all electrons in the bunch are within the right phase of the RF bucket. This is required for proper acceleration by the first X-band structure, without the undesired increase of energy spread and bunch length at the exit of the accelerating structure. The use of a 100 keV injector creates an additional complication: the CLIC accelerating structures are designed for injection with highly relativistic electrons and will reject and even return the 100 keV electron bunches towards the entrance of the X-band structure rather than accelerating them towards the exit. Consequently, the X-band CLIC accelerating structure has to be redesigned so that it accepts the 100 keV electrons for further acceleration.

CLIC accelerating structures are rather short and typically consist of 24 cells to maintain a constant electric field of 100 MV/m throughout the full length of the accelerating structure. To maintain this high gradient while keeping the apertures large enough toward the end of the X-band structure, half of the RF power is dumped into the load at the output coupler of the X-band structure [22]. It was decided to extend the X-band structure for Smart*Light to 50 cells instead of the standard 24 cells for multiple reasons:

- The klystron power is used more efficiently, with only one-fourth of the RF power being dumped at the load.
- Electrons can be accelerated to higher energies using only a single klystron.
- A constant on-axis electric field is not required, and some attenuation of this field towards the end of the X-band structure is acceptable.
- The total length of the X-band structure can still be kept within 0.5 m.

A collaboration with CERN was established to design and manufacture such an *X-band* accelerating structure (100XS50) for the *Smart*Light* project with *50* cells and a low-beta front end for *100* keV electron injection.

2.1.2 Optimization and RF design of the X-band structure

The design of the 100XS50 X-band structure is based on the (*Tapered*) X-band T24 accelerating structure. The T24 structure, designed at CERN for the CLIC project, has a phase advance of 120 degrees per cell and operates at a frequency of 11.9942 GHz [23–25]. This structure consists of an in- and output coupler for RF power at the beginning and the end of the structure with 24 accelerating cells in between. Together, they form a constant gradient accelerating structure.

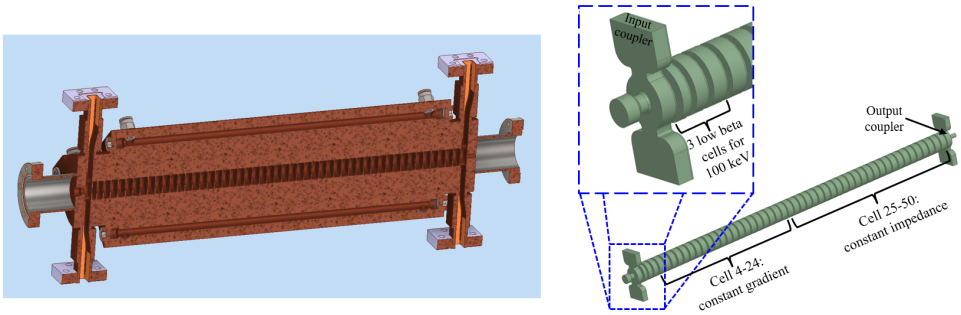

Fig. 3 Left: Cross section of the mechanical design of the hybrid 100XS50 X-band structure. Right: The final inner vacuum (RF) design of the 100XS50, designed using HFSS simulations.

Initially, the dimensions of the apertures of the T24 were copied for the 100XS50 design. This includes the length of each cell together with the diameter, thickness, and radius of the apertures. In the first phase of the Smart*Light project, only a single 10 pC electron bunch per RF pulse will be accelerated and wakefield effects are expected to be minimal. The charged particle tracking code GPT [26], showed that a $Q = 10$ pC electron bunch created by a 100 fs laser pulse on the cathode in combination with a 1.5 GHz compression cavity and a solenoid before and after the cavity (see Fig. 2), can focus the electron bunch at the entrance of the X-band structure at a distance $z = 0.7$ m from the cathode, to a spot size of $\sigma_{\mathrm{r}} \approx 0.3$ mm with a bunch length of $\sigma_{\mathrm{t}} \approx 2$ ps and a normalized emittance of $\epsilon_n \approx 0.55\ \mu\mathrm{m} \cdot \mathrm{rad}$. The length of the input coupler cell and the length of the first 3 cells were optimized to efficiently capture and accelerate such 100 keV electron bunches.

To find the optimized cell lengths, field maps of the on-axis complex electric field in z-direction (propagation direction of the electrons) were created for different cell lengths. To create such field maps, the procedure was followed as described by Schaer et al. in [27]. The on-axis electric field of a cell with length $l_c + \Delta l_c$ can be approximated by scaling the z-positions of the original fieldmap of a cell with length l_c to:

$$s_{\mathrm{str}} = s + \frac{\Delta l_c}{2}\left[1 - \cos\left(\frac{\pi s}{l_c}\right)\right] \tag{4}$$

where s is the original z-position of the fieldmap and s_{str} is the adjusted z-position. The complex on-axis electric field of the T24, with cell of length of 8.332 mm, was used as original field map. The lengths of the matching cell inside the input coupler and the first three cells were adjusted in steps of 100 μm. For each adjustment, the associated fieldmap was created and subsequently used to perform beam dynamics simulations using the GPT code. By field expansions of this generated fieldmap, the complete 3D electromagnetic fieldmap is reconstructed and used in the GPT code. The GPT output of the electron bunch at the exit of the accelerating structures was analyzed for each single fieldmap to find the optimized lengths of the cells.

For this optimization process, several electron bunch parameters at the exit of the X-band structure were taken into account with the purpose of maximizing the

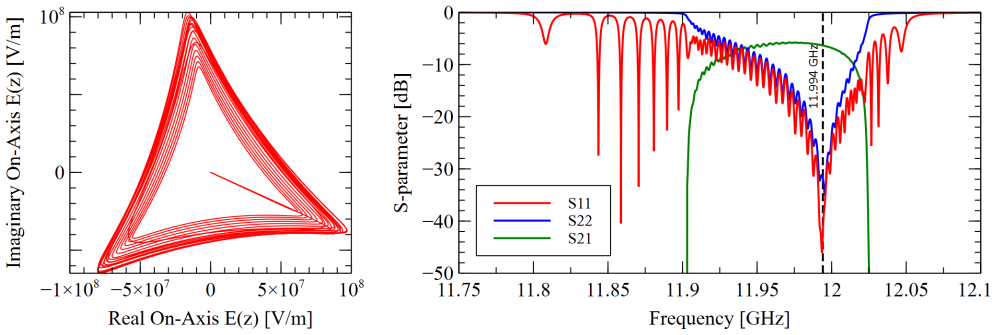

Fig. 4 Left: HFSS simulation of the real- and imaginary components of the on-axis E(z) field along the X-band structure axis. Right: Simulated S-parameters vs frequency.

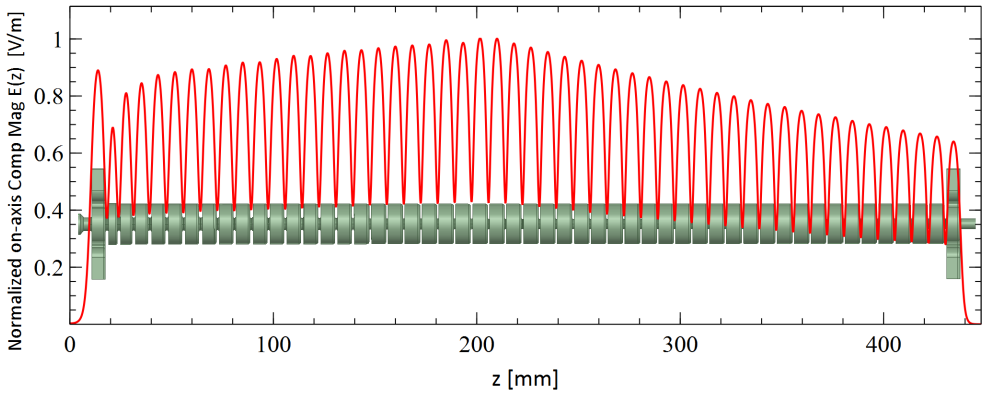

Fig. 5 HFSS simulation of the magnitude of the complex on-axis electric field along the axis of the X-band structure. Cell 1-3: low beta matching cells, cell 4-24: constant gradient, cell 25-50: constant impedance.

number of photons produced by the ICS process while maintaining narrow-band x-rays. Hence, all injected electrons must be accelerated while minimizing the energy spread and bunch length at the exit of the X-band structure. To further maximize the photon production at the ICS interaction point, both the laser pulses and electron bunches need to be focused into a small radial spot size (see Eq. (3)), with typically σ_e a few μm. This requires a low normalized emittance of the accelerated electron bunches. Moreover, for operational stability of the system, preference is given to a combination of cell lengths where the kinetic energy, energy spread, bunch length, and normalized emittance of the accelerated electrons are stable over a broad range of the RF phases of the X-band structure (few tens of degrees). GPT simulations showed that the optimized length of the matching cell in the input coupler had to remain unchanged, while the length of cells one, two and three has to be reduced, respectively, by 2.5 mm, 1 mm and 0.5 mm.

To further increase the electron energy to the required $E_{\mathrm{kin}} \approx 30$ MeV, 26 additional cells were added to the design of the X-band structure. To minimize the effects of radial electric fields in the X-band structure on the electron bunch, the outer electrons should not pass too close to the apertures. Therefore, the diameters of the apertures of the extra cells are kept constant instead of being further tapered towards the end of the X-band structure. As a result, the 100XS50 is a hybrid X-band structure that consists of an input coupler and an output coupler with three low-beta cells, 21 constant gradient cells, and 26 constant impedance cells in between (see Fig. 3).

Table 1 RF properties of the 100XS50 X-band accelerating structure

Operating frequency	11.9942	GHz
Operating temperature	40	°C
Phase advance per cell	120	degree
No. of accelerating cells	50+2	cells+couplers
Total length of structure (including vacuum flanges)	508	mm
Low beta-cells	1-3	cell
Constant gradient cells	4-24	cell
Constant impedance cells	25-50	cell
Group velocity	1.73 - 0.917	%c
Q_0	4947 - 7064	
t_{fill}	135	ns
Electron acceleration at $P_{in} = 24$MW	30.5	MeV

The radius of each separate cell is tuned in HFSS [28] for a phase advance of 120 degrees at an operating frequency of $f = 11.9942$ GHz. The input and output coupler are optimized to minimize S_{11} (see Fig. 4) and to minimize reflections at the output coupler back into the X-band structure and, as such, to eliminate standing waves inside the X-band structure. In Fig. 5, the results of HFSS simulations of the magnitude of the on-axis complex electric field versus z-position in the X-band structure are given. The electric field in the low beta cells decreases with decreasing cell length. The transition from constant gradient to constant impedance is clearly visible. An overview of the RF parameters of the 100XS50 X-band structure is given in Table 1.

Beam dynamics simulations in GPT were done with the optimized 3D electromagnetic fieldmaps, generated by HFFS. 24 MW of RF input power was used in the X-band structure in combination with a solenoid to focus the electron bunch into the ICS interaction point at a distance of 2.2 m from the cathode. Optimization of these beam dynamics simulations showed that a 10 pC electron bunch can be accelerated to an energy of $E_{\mathrm{kin}} = 30.5$ MeV with an energy spread of $\sigma_{E,\mathrm{kin}} = 0.2$ MeV. The bunch can be focused in the interaction point to a radial spot size of $\sigma_{\mathrm{e}} \approx 20\mu$m with a bunch length of $\sigma_{\mathrm{t}} \approx 570$ fs and a normalized emittance of $\epsilon_n \approx 0.63\ \mu\mathrm{m} \cdot \mathrm{rad}$. To optimize the amount of produced x-ray photons in the ICS interaction point, the electron bunch has to be as small as possible in the radial direction (see Eq. (3)). By using a quadrupole triplet instead of a solenoid, the bunch can be further focused to a radial size of $\sigma_{\mathrm{e}} \approx 5\ \mu$m. In the first experiments a solenoid will be used, which will eventually be replaced by a custom made quadrupole triplet.

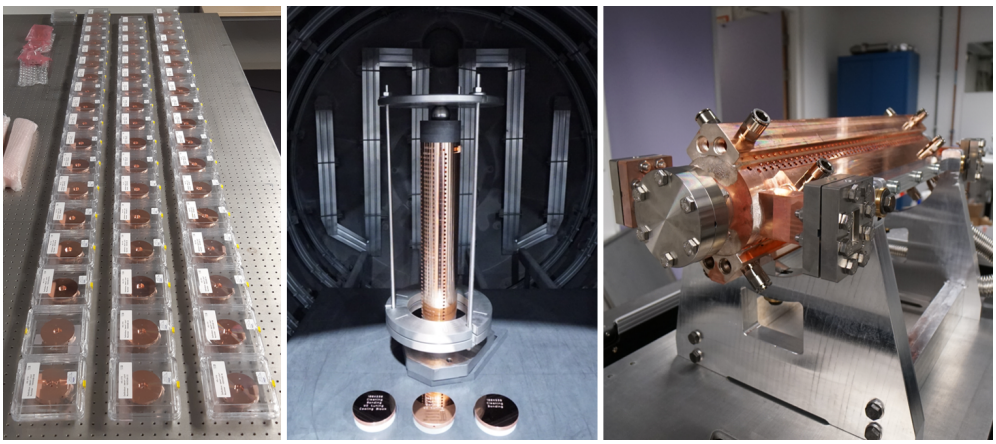

Fig. 6 Left: Separate copper disks with cells and couplers inside the disks. Middle: Stacked and aligned disks in the oven just before the bonding process together with 3 'witness disks'. Right: Accelerator after complete production process.

The energy of the electron bunch – and therefore directly the x-ray energy (see Eq. (2)) – can be easily and quickly changed by adjusting the RF input power of the X-band structure. In the range of 8 to 24 MW RF input power, the energy of the electrons range from 18 to 30 MeV while the other electron bunch parameters can be kept relatively constant in the interaction point by adjusting the focal strength of the focusing solenoid accordingly. This translates into an adjustable x-ray energy from approximately 7 keV to 25 keV.

2.2 Manufacturing and tuning

The cells and couplers have been machined from oxygen-free copper disks with an outer diameter of 80 mm. Each disk is provided with 4 tuning pins rotated by 90 degrees. The high-precision single-point diamond turning of the cells and the milling of the couplers was carried out by VDL ETG [29] with an accuracy better than 1μm (see Fig. 6, left). The assembly of the X-band structure (see the middle picture of Fig. 6) was carried out at Bodycote [30] in close collaboration with the CLIC team. The copper disks were stacked with an accuracy of 4 μm throughout the entire structure before entering the oven. After the bonding process an accuracy of 8 μm was achieved. The standard CLIC technique of diffusion bonding in a vacuum oven at a temperature of 1040 °C with a 20 mbar hydrogen background pressure was used to join the copper disks [31]. Water cooling channels, tuning studs, vacuum tubes, and RF waveguides were brazed to the structure at a lower temperature to form the final 100XS50 X-band structure, as is shown in Fig. 6, right.

Tuning of the structure was carried out at CERN following their standard procedure [32]. The on-axis electric field profile was measured by bead-pull measurements

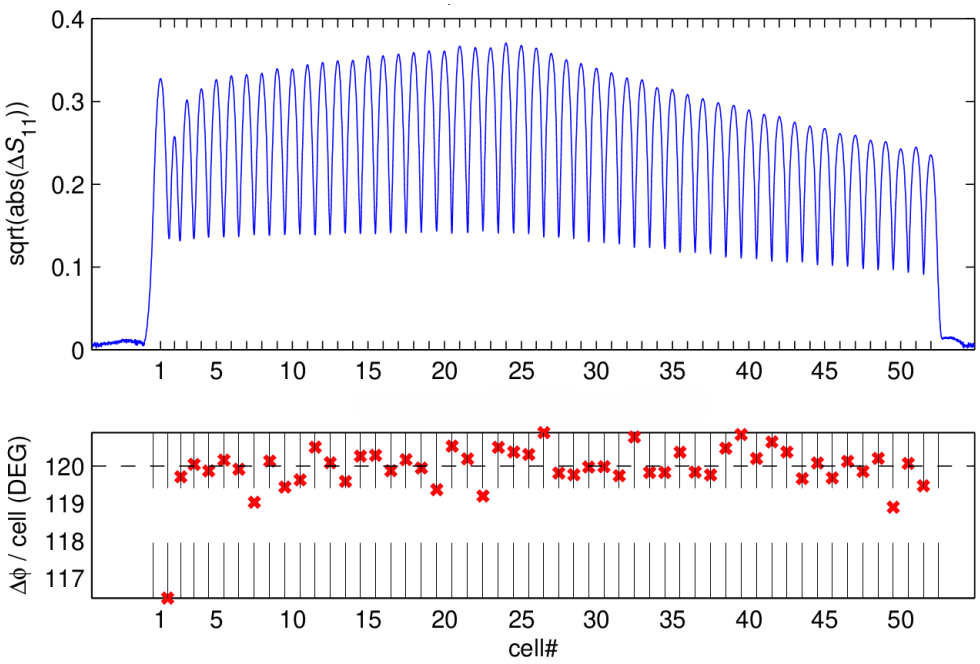

Fig. 7 Measured on-axis electric field profile (top) and phase advance between cells (bottom) after tuning, derived from bead-pull measurement.

and the phase advance between cells was measured to be $120 \pm 1°$ (Fig. 7). The structure is well-tuned with $S_{11} = -53\,\mathrm{dB}$ and $S_{21} = -6.3\,\mathrm{dB}$ and agrees very well with the HFSS simulation (see Fig. 4 and 5).

3 High-power RF conditioning

After manufacturing and tuning, the X-band structure was installed in the *Smart*Light* beamline and connected to the high power RF system through the waveguide network. The main challenge before operation can begin, is the conditioning of the high-power RF system, including the X-band structure. Currently, the conditioning process is still in process.

The X-band structure is driven by a Canon E37123 klystron, which features a double RF window to protect the filament and operates at an X-band RF frequency of 11.9442 GHz, a peak power of 6 MW and a maximum pulse length of 4 μs with an envisioned repetition rate of 500 Hz. The pulsed power to the klystron is delivered by a Scandinova K200 modulator. The RF peak power is increased using a SLED-I RF pulse compressor to reach a maximum power of 24 MW with a pulse length of 200 ns (not taking into account waveguide losses). A detailed description of the RF system can be found in [16, 33].

First the klystron was conditioned separately. After this, the klystron was connected to the full RF system, in particular the pulse compressor and X-band structure.

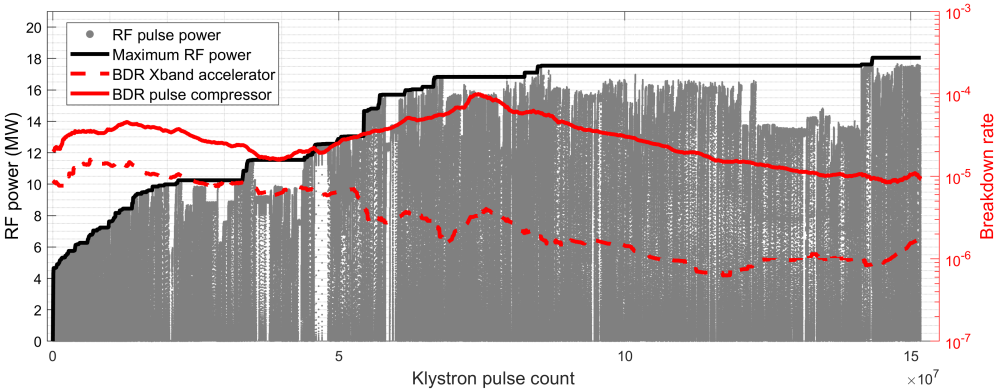

Fig. 8 Peak RF power and breakdown rate (BDR) as a function of pulse count.

In Fig. 8 a graphical overview is presented of the entire conditioning process of the complete system up to now. The peak RF power of individual pulses (gray dots) in the X-band structure is plotted as a function of pulse count. Additionally, the black solid curve indicates the highest power achieved as a function of pulse count. Moreover the breakdown rates (BDR) of the pulse compressor (red solid curve) and X-band structure (red dashed curve) are plotted, which are the result of a moving average of 10^6 RF pulses. The breakdown rates are determined by monitoring the vacuum spikes associated with breakdown events. The breakdown location is attributed to either the pulse compressor or the X-band structure by comparing the relative heights of the vacuum spikes as measured by local vacuum gauges. After 150 million RF pulses we achieved stable operation at a peak RF power of 18 MW at a repetition rate of 50 Hz. The compressed RF pulse length is 200 ns.

4 Electron bunch energy determination by ICS x-ray generation

At the time of writing, the conditioning process was still ongoing but already at a level which is sufficient to accelerate electrons and produce hard x-rays by ICS. Below we present an example of a measurement of ICS-generated x-rays, which also allows us to determine the electron bunch energy and energy spread and thus the performance of the accelerator. These results are discussed in more detail in a forthcoming publication [11].

Electrons were accelerated using 10 MW, 200 ns compressed RF pulses. The electron bunches were focused to a spot size of $\sigma_e \approx 20$ μm in the interaction point, where they collided with the 800 nm femtosecond laser pulses, resulting in a narrow beam of x-rays, propagating in the same direction of the electron beam. The angular distribution of the x-rays was measured as an intensity pattern, using a 4-quadrant MediPix detector [34], as is shown in figure 9 (right). The MediPix detector was placed 1.2 m from the interaction point, corresponding with an opening angle of 24 mrad. The angular pattern reveals features that are characteristic of ICS, such as the γ^{-1} cone

and the asymmetry originating from the laser polarization [11]. Figure 9 (left) shows the corresponding x-ray spectrum, measured using a hyperspectral x-ray camera [35]. The spectrum features the characteristic asymmetric shape of a steep, high-energy Compton edge and a low-energy tail. According to Eq. (1), the measured peak energy at 10.7 keV corresponds to a Lorentz factor of $\gamma = 41.5$ and an electron energy of $E_{\mathrm{kin}} = 20.7$ MeV. Since the final electron energy $E_{\mathrm{kin}} \propto \sqrt{P}$, where P is the RF power, this result can be extrapolated to an electron energy at 24 MW of $E_{\mathrm{kin}} = 32$ MeV. This is in good agreement with the design parameters, shown in Tab. 1.

The relative energy spread of the x-rays $\sigma_{E,\mathrm{x}}/E_{\mathrm{x}}$ is mainly determined by three contributions: one due to the relative laser energy spread σ_λ/λ, one due to the relative electron energy spread σ_γ/γ, and and one due to the electron beam divergence $\sigma_{\theta,e}$, and is given by [36]

$$\sigma_{E,\mathrm{x}}/E_{\mathrm{x}} \simeq \sqrt{(\sigma_\lambda/\lambda)^2 + (2\sigma_\gamma/\gamma)^2 + (\gamma^2\sigma_{\theta,e}^2)^2}. \tag{5}$$

Since the electron beam divergence term only contributes to the low energy tail of the X-ray spectrum and the laser energy spread is known: $\sigma_\lambda/\lambda \approx 5\%$; the electron energy spread $\sigma_{E,\mathrm{kin}}$ can be determined from the width of the high-energy Compton edge. We thus find $\sigma_{E,\mathrm{kin}} \approx 0.13$ MeV, in approximate agreement with the GPT simulations discussed in Sect. 2.1.2.

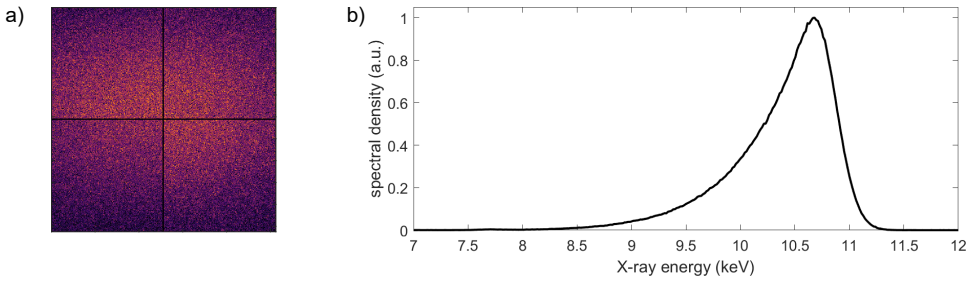

Fig. 9 Left: X-ray intensity distribution generated by ICS, measured with a 4-quadrant MediPix camera. Right: The corresponding measured X-ray spectrum. The Medipix was placed 1.2 m from the interaction point.

5 Conclusion

A compact X-band structure has been designed, manufactured and commissioned that can efficiently accelerate low-energy electron bunches from a 100 keV DC photogun to highly relativistic energies. The high-energy electron bunches will be used to generate x-rays by inverse Compton scattering. The X-band structure has been designed to achieve optimal electron bunch parameters at the electron-laser interaction point. The system has been conditioned up to 18 MW at a repetition rate of 50 Hz. The first x-rays

have been generated, allowing for precise determination of the energy of the accelerated electron bunches and their energy spread. The measured values are in agreement with particle tracking simulations based on the accelerator design. The combination of the X-band structure and the 100 keV DC electron source allows for a compact, narrow-band, and tuneable ICS x-ray source that can operate at a high repetition rate. This opens the way to affordable lab-based ICS x-ray sources of sufficient brilliance for a wide range of applications.

References

[1] The circles of light. Nat. Rev. Mater **3**, 281–282 (2018)

[2] Behling, R.: Modern Diagnostics X-ray Sources. CRC Press, Taylor & Francis Group, 6000 Broken Sound Parkway NW, Suite 300, Boca Raton (2015)

[3] Dreier, T., Nilsson, D., Espes, E.: In-line and at-line battery ct enabled by metaljet sources. In: 13th Conference on Industrial Computed Tomography (iCT), pp. 6–9 (2023)

[4] Zan, G., Vine, D.J., Spink, R.I., Yun, W., Wang, Q., Wang, G.: Design optimization of a periodic microstructured array anode for hard x-ray grating interferometry. Physics in Medicine & Biology **64**(14), 145011 (2019)

[5] Graves, W.S., Bessuille, J., Brown, P., Carbajo, S., Dolgashev, V., Hong, K.-H., Ihloff, E., Khaykovich, B., Lin, H., Murari, K., Nanni, E.A., Resta, G., Tantawi, S., Zapata, L.E., Kärtner, F.X., Moncton, D.E.: Compact x-ray source based on burst-mode inverse compton scattering at 100 khz. Physical Review Accelerators and Beams **17**, 120701 (2014)

[6] Stragier, X.F.D., Mutsaers, P.H.A., Luiten, O.J.: Smart*light: A tabletop, high brilliance, monochromatic and tunable hard x-ray source for imaging and analysis. Microscopy and Microanalysis 24 (Suppl 2), 2018 **24 (Suppl. 2)**, 310–311 (2018)

[7] Graves, W.S.: Results from CXLS commissioning. Paper presented at the 32nd Linear Acceleration Conference (LINAC2024), Chicago, Illinoius, 25–30 August 2024 (2024)

[8] Tilton, S., Eckrosh, K., Larsen, R., Ros, E., Lee, H.S., Valentin, D., Adamo, E., Sandhu, A., Banerjee, S., Kaindl, R., *et al.*: Laser systems and diagnostics for the asu compact x-ray source. In: Compact EUV & X-ray Light Sources, pp. 2–2 (2024). Optica Publishing Group

[9] Günther, B., Gradl, R., Jud, C., Eggl, E., Huang, J., Kulpe, S., Achterhold, K., Gleich, B., Dierolf, M., , Pfeiffera, F.: The versatile x-ray beamline of the munich compact light source: design, instrumentation and applications. Journal of Synchrotron Radiation **27**(7), 1395–1414 (2020)

[10] Dupraz, K., Alkadi, M., Alves, M., Amoudry, L., Auguste, D., Babigeon, J.-L., Baltazar, M., Benoit, A., Bonis, J., Bonenfant, J., *et al.*: The thomx ics source. Physics Open **5**, 100051 (2020)

[11] Elk, I.J.M., Sweers, C.W., Nijhof, D.F.J., Berg, R.G.W., Lucas, T.G., Stragier, X.F.D., Tack, P., Boone, M.N., Luiten, O.J., Mutsaers, P.H.A.: First x-rays from a compact and tunable LINAC-based Compton scattering source (2025). https://arxiv.org/abs/2504.11897

[12] Official CLIC website. https://clic-study.web.cern.ch/. Accessed: 2025-03-16

[13] Brunner, O., Burrows, P., Calatroni, S., Lasheras, N.C., Corsini, R., d'Auria, G., Doebert, S., Faus-Golfe, A., Grudiev, A., Latina, A., et al.: The clic project. arXiv preprint arXiv:2203.09186 (2022)

[14] Aicheler, M., Burrows, P., Draper, M., Garvey, T., Lebrun, P., Peach, K., Phinney, N., Schmickler, H., Schulte, D., Toge, N.: A multi-tev linear collider based on clic technology: Clic conceptual design report. Technical report, SLAC National Accelerator Lab., Menlo Park, CA (United States) (2014)

[15] Catalán Lasheras, N., Argyropoulos, T., Esperante Pereira, D., Eymin, C., Giner Navarro, J., McMonagle, G., Rey, S., Solodko, A., Syratchev, I., Volpi, M., *et al.*: Commissioning of xbox-3: A very high capacity x-band test stand. (2017). The Joint Accelerator Conferences Website (JACoW)

[16] Nijhof, D.F.J.: Ultracold electron source development and x-band acceleration for a compact ics-based x-ray source. PhD thesis, Eindhoven University of Technology (2024)

[17] Oudheusden, T.: Electron source for sub-relativistic single-shot femtosecond diffraction. PhD thesis, Eindhoven University of Technology (2010)

[18] Van Oudheusden, T., De Jong, E., Geer, S., Root, W., Luiten, O., Siwick, B.: Electron source concept for single-shot sub-100 fs electron diffraction in the 100 kev range. Journal of Applied Physics **102**(9) (2007)

[19] Van Oudheusden, T., Pasmans, P., Van Der Geer, S., De Loos, M., Van Der Wiel, M., Luiten, O.: Compression of subrelativistic space-charge-dominated electron bunches for single-shot femtosecond electron diffraction. Physical review letters **105**(26), 264801 (2010)

[20] Pasmans, P., Van Vugt, D., Van Lieshout, J., Brussaard, G., Luiten, O.: Extreme regimes of femtosecond photoemission from a copper cathode in a dc electron gun. Physical Review Accelerators and Beams **19**(10), 103403 (2016)

[21] Pasmans, P.L.E.M.: Ultrafast electron diffraction: An investigation of fundamental limits. PhD thesis, Eindhoven University of Technology (2014)

[22] Argyropoulos, T., Catalan-Lasheras, N., Grudiev, A., Mcmonagle, G., Rodriguez-Castro, E., Syrachev, I., Wegner, R., Woolley, B., Wuensch, W., Zha, H., *et al.*: Design, fabrication, and high-gradient testing of an x-band, traveling-wave accelerating structure milled from copper halves. Physical Review Accelerators and Beams **21**(6), 061001 (2018)

[23] Zennaro, R., Grudiev, A., Riddone, G., Samoshkin, A., Wuensch, W., Tantawi, S., Wang, J., Higo, T.: Design and fabrication of clic test structures. In: Proceedings of LINAC08 (2008)

[24] Higo, T., Higashi, Y., Matsumoto, S., Yokoyama, K., Doebert, S., Grudiev, A., Riddone, G., Wuensch, W., Zennaro, R., Adolphsen, C., et al.: Advances in x-band tw accelerator structures operating in the 100 mv/m regime. THPEA013, IPAC10, Kyoto (2010)

[25] Millar, W.L., Grudiev, A., Wuensch, W., Lasheras, N.C., McMonagle, G., Zennaro, R., Craievich, P., Bopp, M., Lucas, T.G., Volpi, M., *et al.*: High-power test of two prototype x-band accelerating structures based on swissfel fabrication technology. IEEE Transactions on Nuclear Science **70**(1), 1–19 (2022)

[26] General Particle Tracer code. https://www.pulsar.nl/gpt. Accessed: 2025-03-16

[27] Schaer, M., Citterio, A., Craievich, P., Reiche, S., Stingelin, L., Zennaro, R.: rf traveling-wave electron gun for photoinjectors. Physical Review Accelerators and Beams **19**(7), 072001 (2016)

[28] Ansys high-frequency structure simulator. https://www.ansys.com/Products/Electronics/ANSYS-HFSS. Accessed: 2025-03-18

[29] VDL ETG. https://www.vdletg.com. Accessed: 2025-03-21

[30] Bodycote. https://www.bodycote.com/. Accessed: 2025-03-21

[31] Dehler, M., Serpico, C., Shi, J., Citterio, A., Lebet, S., D'Auria, G., Zennaro, R., Gudkov, D., Riddone, G., Atieh, S.: Fabrication of the cern/psi/st x-band accelerating structures. In: International Particle Accelerator Conference (2011)

[32] Shi, J., Grudiev, A., Wuensch, W.: Tuning of x-band traveling-wave accelerating structures. Nuclear Instruments and Methods in Physics Research Section A: Accelerators, Spectrometers, Detectors and Associated Equipment **704**, 14–18 (2013)

[33] Lucas, T., Mutsaers, P., Doorn, H., Heuvel, H., Setten, F., Sluis, M., Stragier, X., Luiten, O.: An overview of the radio-frequency system for an inverse compton x-ray source based on clic technology. In: International Particle Accelerator Conference (2021)

[34] Amsterdam Scientific Instruments (ASI) https://amscins.com/product/cheetah-series (2025). https://amscins.com/product/cheetah-series

[35] Boone, M.N., Assche, F.V., Vanheule, S., Cipiccia, S., Wang, H., Vincze, L., Hoorebeke, L.V.: Full-field spectroscopic measurement of the x-ray beam from a multilayer monochromator using a hyperspectral x-ray camera. Journal of Synchrotron Radiation **27**, 110–118 (2020) https://doi.org/10.1107/S1600577519015212

[36] Mușat, V., Latina, A., D'Auria, G.: A high-energy and high-intensity inverse compton scattering source based on compactlight technology. In: Photonics, vol. 9, p. 308 (2022). MDPI